

Document downloaded from:

<http://hdl.handle.net/10251/144076>

This paper must be cited as:

Rodrigo Bort, M.; Climent, AM.; Liberos Mascarell, A.; Hernández-Romero, I.; Arenal, A.; Bermejo, J.; Fernández-Avilés, F.... (03-2). Solving Inaccuracies in Anatomical Models for Electrocardiographic Inverse Problem Resolution by Maximizing Reconstruction Quality. *IEEE Transactions on Medical Imaging*. 37(3):733-740.
<https://doi.org/10.1109/TMI.2017.2707413>



The final publication is available at

<https://doi.org/10.1109/TMI.2017.2707413>

Copyright Institute of Electrical and Electronics Engineers

Additional Information

Solving inaccuracies in anatomical models for electrocardiographic inverse problem resolution by using electrical information

Miguel Rodrigo, Andreu M. Climent, Alejandro Liberos, Ismael Hernández-Romero, Angel Arenal, Javier Bermejo, Francisco Fernández-Avilés, Felipe Atienza and Maria S. Guillem

Abstract—Electrocardiographic Imaging (ECGI) has become an increasingly used technique for non-invasive diagnosis of cardiac arrhythmias, although the need for medical imaging technology to determine the anatomy hinders its introduction in the clinical practice. This work explores the ability of a new metric based on the inverse reconstruction quality for the location and orientation of the atrial surface inside the torso. Body surface electrical signals from 31 realistic mathematical models and four AF patients were used to estimate the optimal position of the atria inside the torso. The curvature of the L-curve from the Tikhonov method, which was found to be related to the inverse reconstruction quality, was measured after application of deviations in atrial position and orientation. Independent deviations in the atrial position were solved by finding the maximal L-curve curvature with an error of 1.7 ± 2.4 mm in mathematical models and 9.1 ± 11.5 mm in patients. For the case of independent angular deviations, the error in location by using the L-curve was $5.8 \pm 7.1^\circ$ in mathematical models and $12.4^\circ \pm 13.2^\circ$ in patients. The ability of the L-curve curvature was tested also under superimposed uncertainties in the 3 axis of translation and in the 3 axis of rotation and the error in location was of 2.3 ± 3.2 mm and $6.4^\circ \pm 7.1^\circ$ in mathematical models, and 7.9 ± 10.7 mm and $10.0^\circ \pm 12.8^\circ$ in patients. The curvature of L-curve is a useful marker for the atrial position and would allow emending the inaccuracies in its location.

Index Terms—Electrocardiographic imaging, heart position, atrial position, inverse methods, L-curve.

I. INTRODUCTION

NONINVASIVE identification of cardiac electrical activity or electrocardiographic imaging (ECGI) has become an increasingly used technique in clinical practice. This technique allows to reconstruct the electrical activity in the whole heart

Submitted by December 20th, 2016. This work was supported in part by: Generalitat Valenciana Grants (ACIF/2013/021); the Instituto de Salud Carlos III (Ministry of Economy and Competitiveness, Spain: PI13-01882, PI13-00903; PI14/00857; TEC2013-46067-R and DTS16/00160); Spanish Society of Cardiology (Grant for Clinical Research in Cardiology 2015) and the Spanish Ministry of Science and Innovation (Red RIC, PLE2009-0152).

M. Rodrigo and M. S. Guillem are from ITACA Institute, Universitat Politècnica de València, Valencia, Spain. (e-mail: mirodbor@upv.es).

A. M. Climent, A. Liberos, I. Hernández-Romero, Angel Arenal, Javier Bermejo, F. Fernández-Avilés and F. Atienza are from Hospital General Universitario Gregorio Marañón, Instituto de Investigación Sanitaria Gregorio Marañón, Madrid, Spain.

I. Hernández-Romero is from Rey Juan Carlos University, Fuenlabrada, Madrid, Spain.

with much higher spatial resolution [with simultaneous signals](#) than invasive techniques currently used, and the potential to simultaneously estimate the electrical signal everywhere in the myocardium has been exploited in the study of both ventricular [1-2] and atrial arrhythmias [3-6].

Electrocardiographic imaging is based on the resolution of the inverse problem of electrocardiography, making use of signals recorded by Body Surface Potential Mapping (BSPM) and the 3D anatomy of the torso and heart of the patients. All this information allows reversing the propagation model between the myocardial tissue and the patient's torso [7]. However, some inaccuracies in these data may appear when the CT/MRI images and the BSPM recordings are not obtained immediately one after another and have to be taken on different days. This delay results in a mismatch in the heart location causing a loss in accuracy in the inverse-computed signals. Moreover, the heart position is subjected to other sources of movement artifacts, like respiration or ventricular contraction [[Jiang](#)].

Tikhonov regularization is one of the methodologies used to solve the inverse problem and its optimization by the L-curve method allows the system to find a balance between the errors committed in the non-invasive signal estimation and the intrinsic numerical error of the inverse solution [7-8]. It has been observed that the worsening of the system conditions, such as the displacement of the heart within the torso, affects the L-curve shape. This paper evaluates whether the measurement of the L-curve deterioration quantified in terms of its curvature allows minimizing the uncertainties on the system conditions, namely the inaccuracies in the atrial position in a population of patients of atrial fibrillation (AF). An automatic method to remove inaccuracies in atrial position would not only allow to obtain better outcomes with non-invasive techniques, but also to expand the use of the ECGI technology to larger cohort of AF patients.

II. MATERIALS AND METHODS

A. Mathematical models

A realistic 3D model of the atrial anatomy composed by 284,578 nodes and 1,353,783 tetrahedrons (673.4 ± 130.3 μm between nodes) was used to simulate the atrial electrical activity [9]. A gradient on the electrophysiological properties

of the atrial myocardium, specifically on $I_{K_{ACH}}$, I_{K1} , I_{Na} and I_{CaL} [10-11], was introduced into the atrial cell formulation [10,12-13] to obtain propagation patterns with varying propagation patterns. The system of differential equations in the atrial cell model was solved by using Runge-Kutta integration based on a graphic processors unit (NVIDIA Tesla C2075 6G) [14]. An ensemble of 31 different AF episodes was simulated with different degrees of complexity (with fibrosis ratios from 0% to 60%) and different patterns of activation rates. Among these models, 14 AF patterns were driven by a single rotor at varying locations of the [left atria \(LA\)](#), [LA \(pulmonary veins \(PV\)\)](#), [PLAW](#) posterior left atrial wall (PLAW) and [left atrial appendage \(LAA\)](#) and [LAA](#) and 17 AF patterns driven by a single rotor at varying locations of the [RA](#) right atria (RA) ([free RA wall](#) free right atrial wall and [RAA](#)) right atrial appendage (RAA)).

For each simulation, a uniform mesh of unipolar [electrograms \(EGMs\)](#) was calculated at 1 mm from the epicardial surface under the assumption of a homogenous, unbounded and quasi-static conducting medium by summing up all effective dipole contributions over the entire model [15]. Computed electrograms were stored for processing at a sampling frequency of 500 Hz.

The ECG potentials on the torso model were calculated by solving the Forward Problem [6] in a mesh formed by 771 nodes and 1538 triangular patches, in which the atrial model was co-located within the torso by using the images from the Visual Human Project [16]. White Gaussian noise was added to the synthetic ECG signals with a signal-to-noise ratio of 30dB.

B. Patient recording

Four patients admitted for ablation of drug-refractory paroxysmal AF (females, 57.2 ± 17.4 years) were included in the study. The protocol was approved by the Institutional Ethics Committee of our institution and all patients gave informed consent.

Multichannel electrocardiograms (ECGs) were recorded with 57 chest ECG leads by using the Body Surface Potential (BSPM) technique [17]. The signals were recorded using a commercial system (Clearsign™ Amplifier, Boston Scientific, Natick, MA) and the 57 electrodes were distributed as follows: 24 electrodes on the anterior, 24 on the posterior, 3 on each lateral side of the torso and 3 extra leads in order to obtain a Wilson Central Terminal. Photographic images from multiple points of view were obtained for each patient wearing the recording electrodes.

The electrophysiological study was performed under general anesthesia and periodic heparin bolus administration. Intracardiac electrograms and atrial anatomy were obtained from both atria during the procedure by using both the ablation catheter (Therapy Cool Path, St. Jude Medical, St. Paul, Minnesota) and the circular mapping catheter (Optima, St. Jude Medical, St. Paul, Minnesota) introduced via the right femoral vein and guided by an electroanatomical navigation system (Ensite NavX System version 8.0 (St. Jude Medical, Minneapolis, Minnesota) that enabled atrial anatomy

reconstruction. Two patients arrived in sinus rhythm and AF was induced using electrical burst pacing [18]. Then, a central venous bolus of adenosine (12-18 mg) was administered in order to produce a significant atrio-ventricular block and to remove the ventricular activation [11]. At peak adenosine effect, ECGs segments surrounding the longest RR interval were used for the analysis. Nineteen AF signal segments from the 4 patients (4.7 ± 3.1 segments per patient) with duration of 5.6 ± 2.1 seconds were used for the analysis. [Baseline of BSPM signals was estimated by decimation to 50 Hz and a posterior filtering with a Butterworth 10th-order low-pass filter with a cut-off frequency of 2 Hz. This signal was interpolated to 2 kHz \(the sample frequency\) and subtracted from the original signal. BSPM signals were then low-pass filtered with a 10th-order Butterworth filter with a cut-off frequency of 40 Hz \[Rodrigo 2014\].](#)

MRI images with a spatial resolution of $0.7 \times 0.7 \times 1.5$ mm were acquired 2-3 days prior to the ablation procedure. Atria and torso anatomy were obtained by segmentation of MRI images by using by using ITK-SNAP [19]. Additionally, the torso anatomy, together with the electrodes location was obtained by processing the conventional photographic images previously acquired [20]. Anatomical models obtained with the different technologies were co-registered by using an algorithm based on rigid transformations [21] guided by 8 points manually marked in both atrial models (4 PVs, LAA, RAA, [superior vena cava \(SVC\)](#) and [inferior vena cava \(IVC\)](#) and [SVC, IVC](#)) or torso models.

C. Inverse solution and L-curve

We estimated the inverse-computed EGM (icEGM) from both patient recordings and mathematical models by computing the inverse of the field transfer atrial-torso matrix:

$$icEGM = M^{-1} \cdot ECG \quad (1)$$

where M is the field transfer matrix between the atria and the torso [7]. Since M is ill-conditioned, its inverse matrix cannot be computed in terms of classical linear algebra. We solved the system by using zero-order Tikhonov's method in which the potentials on the surface of the atria $icEGM$ were estimated from the potentials on the torso according to equation (2) [6,8, [Figueras](#)].

$$icEGM(\lambda) = (M^t \cdot M + \lambda \cdot I^t \cdot I)^{-1} \cdot M^t \cdot ECG \quad (2)$$

where I is the identity matrix and λ is [the a constant regularization parameter that does not depend on time](#). The optimal regularization parameter was selected according to the L-curve method, which choses the corner of the error norm ($\|M \cdot icEGM(\lambda) - ECG\|^2$) vs. the solution norm ($\|icEGM(\lambda)\|^2$) for the different regularization parameters (see Fig. 1), [being the operator \(\$\|\cdot\|\$ \) the Frobenius norm](#). This corner of the L-curve minimizes the expression $\|M \cdot icEGM(\lambda) - ECG\|^2 + \lambda^2 \|icEGM(\lambda)\|^2$ and provides the $icEGM$ solution that best satisfies equation (1) and minimizes the extreme values on the solution that can be mostly

attributed to the numerical errors involved in the transfer matrix inversion [7]. The corner of the L-curve was defined as the maximum curvature point according to (3):

$$curvature(\lambda) = \frac{\frac{dx}{d\lambda} \frac{d^2y}{d\lambda^2} - \frac{dy}{d\lambda} \frac{d^2x}{d\lambda^2}}{\left[\left(\frac{d^2x}{d\lambda^2} \right)^2 + \left(\frac{d^2y}{d\lambda^2} \right)^2 \right]^{3/2}} \quad (3)$$

where x was the logarithm of the error norm ($\log\|M \cdot icEGM(\lambda) - ECG\|^2$) and y the logarithm of the solution norm ($\log\|icEGM(\lambda)\|^2$). The optimal regularization parameter was chosen at the first local maximum value of the curvature.

The basis of the atrial location identification based on the L-curve shape is shown in Fig. 1E. It can be observed that the L-curve calculated for the right location shows a sharp corner whereas the L-curve computed for an incorrect location of the atria is smoother and, therefore, the curvature is higher for the correct location than for the displaced location (4.53 vs 0.43).

D. Estimation of the location of the atria based on L-curve shape

Description of the experiments

In order to explore the potential use of the L-curve shape to estimate the location of the atria inside the thorax we varied the location and orientation of the atria both in our mathematical models and in our patient data and computed the maximum L-curve curvature under all tested model alterations.

In Fig. 1, a sample case of the resolution of the inverse problem of electrocardiography with a modification in the model geometry is represented. The forward problem was solved with the atria at the “original location” and then the inverse problem was solved both for the atria at the original and “displaced” location (5 cm distance). With the departing EGMs (Fig. 1.A), a rotor can be identified in the right atrial wall. In this case, inverse-computed phase maps calculated with the same geometries for the forward and inverse calculations do allow to identify the rotor at the same location, despite the differences that can be observed both in potential and phase maps, as shown in Fig. 1.C. However, inverse-computed maps obtained with a displacement in the atrial location (Panel D), no longer allow the identification of the atrial rotor.

The basis of the atrial location identification based on the L-curve shape is shown in Fig. 1E. It can be observed that the L-curve calculated for the right location shows a sharp corner whereas the L-curve computed for an incorrect location of the atria is smoother and, therefore, the curvature is higher for the correct location than for the displaced location (4.53 vs 0.43).

In order to assess the ability of the L-curve curvature for solving the spatial inaccuracies in the atrial surface location, several tests were performed. In mathematical simulations, we used the EGM potentials from the atria on its proper position to calculate the BSPM on the virtual torso. Then, these BSPM signals were used to calculate the L-curve under deviations in the atrial locations. In patients, we used the recorded BSPM signals to obtain the L-curve under deviation from the original

position of the atria, extracted from the MRI scan.

The ability of the L-curve curvature to identify the proper position of the atria under such deviations was studied as follows:

- First, single deviations—displacements in every axes X, Y and Z. It was (displacements or rotations) were evaluated in a subset of 10 mathematical models (10 different models for each axis, Figures 2.A and S1) models—and in the whole patient population (Figure 2.B and S2) by measuring the L-curve curvature in presence of gradual—gradual deviations—displacements in each of the axes.
- Single rotations in axes X, Y and Z. It was evaluated in a subset of 10 mathematical models (10 different models for each axis, Figures 3.A and S3) and in the whole patient population (Figures 3.B and S4) by measuring the L-curve curvature in presence of gradual rotations in each of the axes.
- Two superimposed rotations: a fixed random deviation in one axis (X) and a gradual deviation in a perpendicular axis (Y). It was evaluated in all mathematical models (Figure S5.A) and in the whole patient population (Figure S6.A) by measuring the L-curve curvature in presence of a fixed random rotation in the X axis (from -30° to 30°) and a gradual rotation in the Y axis. Each simulation/patient had a different random rotation in X axis which was preserved along the gradual changes in the Y axis.
- Three superimposed rotations: a fixed random deviation in two axes (X and Y) and a gradual deviation in a perpendicular axis (Z). It was evaluated in all mathematical models (Figure S5.B) and in the whole patient population (Figure S6.B) by measuring the L-curve curvature in presence of a fixed random rotation in the X and Y axes (from -30° to 30°) and a gradual rotation in the Z axis. Each simulation/patient had a different random rotation in X and Y axes which was preserved along the gradual changes in the Z axis.
- Inaccuracies in all axes: the atrial surface had a random angular deviation in the three axes (X, Y and Z) and a displacement in the 3 axes. It was evaluated in all mathematical models (Figure 4.A) and in the whole patient population (Figure 5.B) by measuring the L-curve curvature in presence of a fixed random rotation in the three axes (from -30° to 30°) and a displacement between 0 and 45 mm in a random direction. Each simulation/patient had a different random rotation in the three axes which was preserved along the gradual changes in displacements.

Then, the whole dataset was evaluated in presence of two superimposed rotations: a fixed random deviation in one axis (X) and a gradual deviation in a perpendicular axis (Y) in which the L-curve curvature was measured. Then, the same experiment was carried out in the presence of three superimposed rotations: two fixed random deviations in two axes

Con formato: Sangría: Izquierda: 0,12 cm, Con viñetas + Nivel: 1 + Alineación: 0,63 cm + Sangría: 1,27 cm

Con formato: Sangría: Izquierda: 0,12 cm

Con formato: Sangría: Izquierda: 0,12 cm, Con viñetas + Nivel: 1 + Alineación: 0,63 cm + Sangría: 1,27 cm

Con formato: Sangría: Izquierda: 0,12 cm

Con formato: Sangría: Izquierda: 0,12 cm, Con viñetas + Nivel: 1 + Alineación: 0,63 cm + Sangría: 1,27 cm

Con formato: Con viñetas + Nivel: 1 + Alineación: 0,63 cm + Sangría: 1,27 cm

(X and Y) and a gradual deviation in a perpendicular axis (Z) in which the L-curve curvature was measured. Finally, the whole dataset was evaluated in presence of inaccuracies in all axes: the atrial surface had a random angular deviation in the three axes (X, Y and Z), and the L-curve curvature was evaluated for several distances from the original position to a random displacement in the three axes.

III. RESULTS

A. Illustrating example

In Fig. 1, a sample case of the resolution of the inverse problem of electrocardiography with a modification in the model geometry is represented. The forward problem was solved with the atria at the "original location" and then the inverse problem was solved both for the atria at the original and "displaced" location (5 cm distance). With the departing EGMs (Fig. 1.A), a rotor can be identified in the right atrial wall. In this case, inverse-computed phase maps calculated with the same geometries for the forward and inverse calculations do allow to identify the rotor at the same location, despite the differences that can be observed both in potential and phase maps, as shown in Fig. 1.C. It can be also observed that the correlation between the original (blue) and the inverse-computed (red) EGM is moderated (0.48), although the reconstructed signal maintains the overall shape. However, inverse-computed maps obtained with a displacement in the atrial location (Panel D), no longer allow the identification of the atrial rotor, and in this case the individual signal shows a lower correlation (0.18) compared with the solution with the atrial anatomy in its proper position.

A-B. Single axis displacement vs. curvature

We first evaluated the curvature of the L-curve for displacements in the location of the atria inside the thorax in each of the X, Y, Z axis for the resolution of the inverse problem (Fig. 2, S1 and S2). For displacements in the X axis of mathematical simulations (Fig. 2.A), the maximum

curvature was found on average for the correct location of the atria. Indeed, 8 simulations showed their maximal curvature for 0 mm of displacement, and 2 simulations for -5 mm. Therefore, in case of an uncertainty in the actual location of the atria inside the thorax in the X axis, it could be estimated with a mean error of 1.0 ± 2.1 mm. Similar observations were made for displacements in the Y and Z axes, with errors in the location of the atria of 3.0 ± 2.6 mm and 1.0 ± 2.1 mm for the displacement in the Y and Z axes, respectively (Fig S1.A-B). Overall, the mean error was 1.7 ± 2.4 mm.

The same experiments were conducted with patient data, in which the location of the atria, obtained my MRI, was altered in each of the X, Y and Z axes (Fig. 2 and S2). Again, the maximum curvatures were obtained at the actual location of the atria inside the thorax. If the location of the atria is defined as that with the largest L-curve corner curvature, then the observed errors were 5.8 ± 5.1 mm, 7.2 ± 8.9 mm and 14.2 ± 16.1 mm for the X, Y and Z axes, respectively (9.1 ± 11.5 mm on

average). By looking at the individual tracings for all the curvature measurements (gray lines), largest curvatures do clustered around the maximum value 0 mm error position. This holds even for those patients in whom the location of the atria by the L-curve curvature and MRI did not match, which may be the consequence of an inaccurate registration of the MRI and the electrodes location by conventional images.

B-C. Single axis rotation vs. curvature

The second stage of the L-curve accuracy assessment was to evaluate its ability to properly detect a rotation in the atria inside the thorax. In Fig. 3, S3 and S4, results of the inverse problem resolution after rotations between -30° and 30° around each of the three axes are presented. In Fig. 3.A the curvatures obtained for each simulation affected by rotations in X axis are depicted, and all of them showed their maximal curvature of the L-curve in the actual location of the atria and, therefore, the error in rotation identification was $0.0 \pm 0.0^\circ$. Rotations in Y axis, however, resulted in no clear trends that may allow the identification of the actual location (Fig. S3.A), with maximum values distributed from -18° to 24° and a location error of $13.8 \pm 6.4^\circ$. Finally, the angular deviation in the Z axis produced an error in the angular location of $3.6 \pm 3.1^\circ$. The overall mean error was $\pm 5.8 \pm 7.1^\circ$.

In Fig. 3.B and S4 show the results from rotations of the atria inside the thorax of AF patients. Fig. 3.B shows the curvatures obtained after rotations around the X axis, which resulted in an error in the estimation of the angular position of the atria of $4.1 \pm 5.1^\circ$. As in the mathematical models, the angular deviation in the Y axis produced a more widespread distribution, as can be observed in Fig. 3.C and S4.A, with an error in the angle detection of $189.35 \pm 15.94^\circ$. Finally, the angular deviation in the Z axis provoked an error of $12.6 \pm 11.9^\circ$ (Fig. 3.C and S4.B) and thus the mean error was $12.4 \pm 13.2^\circ$.

C-D. Combined rotations and displacements vs. curvature

Since errors in location and orientation of the atria inside the thorax can appear in combination, we then evaluated the potential use of the L-curve curvature for identifying these errors in a step-wise manner. For each of the mathematical models random rotations in the X, Y and Z axes (-30° to 30°) were applied and then we evaluated the curvature of the L-curve as a function of the distance from the actual location of the atria inside the thorax (0 to 45 mm, Fig. 4.A). It can be observed that the curvature showed its maximum values in the vicinities of the actual location, resulting in an error in the position estimation of 2.3 ± 3.2 mm. In patients, errors in the location of the atria inside the thorax under random rotations in the 3 axes were 7.9 ± 10.7 mm (Fig. 4.B).

Furthermore, the ability of the proposed method to orientate the atria in its actual position when simultaneous rotations in 2 or 3 axes are present was evaluated. For that purpose, a random rotation in the X axis was applied (-30° to 30°) and then the curvature was evaluated for rotations in the Y axis

Con formato: Normal, Justificado

Con formato: Sangría: Primera línea: 0,36 cm

(Fig. S5.A and S6.A). Again, rotations around the y -Y axis showed a widespread distribution of curvatures but even in this scenario, the error in the angular deviation identification was $8.9 \pm 7.6^\circ$ for mathematical models and $18.4 \pm 14.6^\circ$ for patients (Fig. 4.C). Finally, a random rotation was applied in the X and Y axes and then the curvature was evaluated for rotations in the Z axis (Fig. S5.B and S6.B). This case showed an error of $6.4 \pm 7.1^\circ$ in the angular deviation identification for mathematical models and $40.12.01 \pm 125.85^\circ$ in patients.

IV. DISCUSSION

This study presents a new approach for refining the location of the atria inside the thorax by solving the inverse problem of electrocardiography based on electrical information, whose validity has been tested both in mathematical models and in patients. The ability of the L-curve curvature for the location and orientation of the atria has been tested under single and multiple combined displacements and rotations. Location errors were found to be < 1 cm, and thus this method could potentially be used in a realistic scenario.

A. Anatomical models and inverse problem resolution

Solution of the inverse problem of electrocardiography generally involves the recording of MRI or CT images for obtaining accurate anatomical models of the patients. These MRI or CT images are obtained with the BSPM electrodes in place so that the geometric parameters are preserved [22]. Although previous works have reported that the inverse problem can overcome to spatial uncertainties up to 1cm with similar results [23], the proper spatial localization and construction of accurate anatomical models offer better outcomes of the inverse solutions [24, Keller, van Dam].

However, it is not always feasible to obtain the MRI together with useful BSPM recordings. This is the case for paroxysmal AF patients that may arrive in sinus rhythm and induction of AF should only be performed in the electrophysiological laboratory. In addition, in order to validate the inverse problem resolution during AF, both BSPM

recordings and invasive data should be obtained simultaneously [25] and cannot be done inside the MRI or CT scanner. In order to overcome the limitations of the inverse problem resolution in AF, we propose to refine the geometry obtained from a prior scan with electrical information, which may allow the use of the inverse problem resolution for paroxysmal AF patients and not only persistent AF patients.

B. The L-curve regularization and anatomical model

The L-curve regularization method has been profusely used in the literature to solve ill-posed systems, as the case of the inverse problem of electrocardiography [7,23,26]. Previous works have reported the sensitivity of the inverse problem to uncertainties on either the signals or the transfer matrix [22-23,27, Huiskamp]. Our work makes use of the change in the L-curve curvature that occurs when there are inaccuracies in the transfer matrix, in our case caused by uncertainties in the

atrial location, which cause significant errors with all possible solutions for all the regularization parameters. In this case, the division between the numerical error and the error on the solution (the two “arms” of the L-curve) is not so abrupt, thus it produces a smothered curvature in the “corner” of the L-curve. However, this is the first work that proposes to take advantage of this property of the L curve in order to refine the geometry of the model.

We have shown that the curvature at the corner of the L curve is maximized for matching forward and inverse problem anatomies. However, this approach seems to be more sensitive for displacements than for rotations and less sensitive for rotations around a main axis of the geometrical model itself (i.e. rotations around the Y axis). Notice that rotations around a main axis of the model do not result in major changes in location since the atria is inscribed roughly in the same volume while rotations around any other axis do result in a change in the occupied volume. This would explain why both in patients and mathematical models the error in atrial rotation having 3-axis angular deviations is lower than the error having just 2-axis angular deviations, since the 2-axis case was measured in the Y axis and the 3-axis case in the Z axis. We have also shown that it is possible to identify the closest location in each axis in a stepwise manner because the curvature is also maximized even if there are unresolved location errors in other axes. Thus, each of the uncertainties (displacements and rotations) could be solved individually and iteratively, first displacements and then rotations, in a stepwise manner.

In our study we used both of human data and mathematical models because the gold standard anatomy has to be estimated from CT images and thus there is some uncertainty about the actual anatomy and the location of electrodes. As expected, results in atrial location and orientation provided better outcomes in mathematical models than in patients, in which there are electrical noise, more complex electrical patterns and more model inaccuracies. In particular, we found larger errors for locating the atria in the Z axis than for the other axis and this was not reproduced in the mathematical models. We attribute this differential effect to model inaccuracies, since the CT image and the conventional image were obtained with the patients at different postures (laying vs. sitting), which may affect the Z axis to a greater extent than the other axes. We believe that validation with a more accurate geometrical model can only be more favorable and thus we are underestimating its accuracy.

C. Limitations and future work

For both patients and mathematical models a simplistic torso conductor volume was considered for the inverse solution, without the inclusion of lungs, blood vessels or bones. This decision is supported by the literature, since the inverse-computed signals have been reported to be slightly affected by the inhomogeneities of the torso volume [22,24,28, Keller, van Dam] in comparison with the effect of changes in the heart position. Although previous studies were carried out on ventricular signals, the study of the forward problem on

atrial signals also reported the relative invariance against the torso inhomogeneities [29-30].

This study used the curvature of the L-curve only for the atrial location and orientation. However, other parameters related to the L-curve shape may also help in determining the best match for geometrical models. Although we found the curvature of the corner of the L-curve to be the most robust indicator, we did not test any combination of L-curve descriptors which may allow an improved performance.

We have shown that the location of the atria can be resolved in a stepwise manner. An exhaustive search in the entire volume may be too computationally intense. However, the accuracy in the location of the atria may be increased if the algorithm was run more than once and thus the location was iteratively refined, since the errors in location or angular deviation are lower when no other inaccuracies are involved.

Finally, the validity of the method has been tested just for AF signals, its extension to other atrial arrhythmias remains unproven. However, AF presents the most complicated electrical pattern that can be found in atrial electrophysiology, and sensible to the low-pass filtering effect of the torso conductor [31]. We believe that the method could be extended to other less complicated rhythms but its reliability for other conditions remains to be tested.

V. CONCLUSION

This work presents a novel technique based on the curvature of the L-curve for placing the atria inside the chest when solving the inverse problem of electrocardiography. The presented technique has been tested for both mathematical models and patients, and under single or multiple uncertainties on the atrial location. It has been shown that this geometrical identification can be achieved with errors of about 1 cm and 15°. This technique could be useful for avoiding the spatial artifacts present in the inverse problem but also to extend the use of this technique by making possible the utilization of previously obtained CT/MRI images of the patient.

REFERENCES

- [1] P. S. Cuculich, J. Zhang, Y. Wang, K. A. Desouza, R. Vijayakumar, P. K. Woodard, Y. Rudy. (2011, Oct.). The electrophysiological cardiac ventricular substrate in patients after myocardial infarction: noninvasive characterization with electrocardiographic imaging. *J Am Coll Cardiol*. [Online]. 130 (7), pp. 530-8. Available: <http://www.sciencedirect.com/science/article/pii/S0735109711028683>
- [2] A. S. Revishvili, E. Wissner, D. S. Lebedev, C. Lemes, S. Deiss, A. Metzner, V. V. Kalinin, O. V. Sopov, E. Z. Labartkava, A. V. Kalinin, M. Chmelevsky, S. V. Zubarev, M. K. Chaykovskaya, M. G. Tsiklauri, K. H. Kuck. (2015, Aug.). Validation of the mapping accuracy of a novel non-invasive epicardial and endocardial electrophysiology system. *Europace*. [Online]. 17 (8), pp. 1282-8. Available: <http://europace.oxfordjournals.org/content/17/8/1282.long>
- [3] M. Haissaguerre, M. Hocini, A. Denis, A. J. Shah, Y. Komatsu, S. Yamashita, M. Daly, S. Amraoui, S. Zellerhoff, M. Q. Picat, A. Quotb, L. Jesel, H. Lim, S. Ploux, P. Bordachar, G. Attuel, V. Meillet, P. Ritter, N. Derval, F. Sacher, O. Bernus, H. Cochet, P. Jais, R. Dubois. (2014, Aug.). Driver domains in persistent atrial fibrillation. *Circulation*. [Online]. 130 (7), pp. 530-8. Available: <http://circ.ahajournals.org/content/130/7/530.long>
- [4] P. S. Cuculich, J. Zhang, Y. Wang, K. A. Desouza, R. Vijayakumar, P. K. Woodard, Y. Rudy. (2011, Oct.). The electrophysiological cardiac ventricular substrate in patients after myocardial infarction: noninvasive characterization with electrocardiographic imaging. *J Am Coll Cardiol*. [Online]. 58 (18), pp. 1893-902. Available: <http://www.sciencedirect.com/science/article/pii/S0735109711028683>
- [5] Y. Wang, R. B. Schuessler, R. J. Damiano, P. K. Woodard, Y. Rudy. (2007, Dec.). Noninvasive electrocardiographic imaging (ECGI) of scar-related atypical atrial flutter. *Heart Rhythm*. [Online]. 4 (12), pp. 1565-7. Available: <http://www.sciencedirect.com/science/article/pii/S1547527107008764>
- [6] J. Pedrón-Torrecilla, M. Rodrigo, A. M. Climent, A. Liberos, E. Pérez-David, J. Bermejo, A. Arenal, J. Millet, F. Fernández-Avilés, O. Berenfeld, F. Atienza, M. S. Guillem. (2016, Apr.). Noninvasive Estimation of Epicardial Dominant High-Frequency Regions During Atrial Fibrillation. *J Cardiovasc Electrophysiol*. [Online]. 27 (4), pp. 435-42. Available: <http://www.ingentaconnect.com/content/bsc/jce/2016/00000027/00000004/art00009>
- [7] B. M. Horáček, J. C. Clements. (2015, Aug.). The Inverse Problem of Electrocardiography: A Solution in Terms of Single- and Double-Layer Sources on the Epicardial Surface. *Math Biosci*. [Online]. 144 (2), pp. 119-54. Available: <http://www.sciencedirect.com/science/article/pii/S0025556497000242>
- [8] A. N. Tikhonov. (1963). On the solution of incorrectly posed problems and the method of regularization. *Sov Math Dokl*. [Journal]. 4, pp. 1035-1038.
- [9] O. Dössel, M.W. Krueger, F.M. Weber, M. Wilhelms, G. Seemann. (2012, Aug.). Computational modeling of the human atrial anatomy and electrophysiology. *Med Biol Eng Comput*. [Online]. 50 (8), pp. 773-99. Available: <http://link.springer.com/article/10.1007%2Fs11517-012-0924-6>
- [10] J. T. Koivumäki, G. Seemann, M. M. Maleckar, P. Tavi. (2012, May). In silico screening of the key cellular remodeling targets in chronic atrial fibrillation. *PLoS Comput Biol*. [Online]. 10 (5), pp. e1003620. Available: <http://journals.plos.org/ploscompbiol/article?id=10.1371/journal.pcbi.1003620>
- [11] F. Atienza, J. Almendral, J. Moreno, R. Vaidyanathan, A. Talkachou, J. Kalifa, A. Arenal, J.P. Villacastán, E.G. Torrecilla, A. Sánchez, R. Ploutz-Snyder, J. Jalife, and O. Berenfeld. (2006, Dec.). Activation of inward rectifier potassium channels accelerates atrial fibrillation in humans: evidence for a reentrant mechanism. *Circulation*. [Online]. 114 (23), pp. 2434-42. Available: <http://circ.ahajournals.org/content/114/23/2434.long>
- [12] M. Courtemanche, R.J. Ramirez, S. Nattel. (1998, Jul.). Ionic mechanisms underlying human atrial action potential properties: insights from a mathematical model. *Am J Physiol*. [Online]. 275 (1 Pt 2), pp. H301-21. Available: <http://ajpheart.physiology.org/content/275/1/H301.long>
- [13] J. Kneller, R.J. Ramirez, D. Chartier, M. Courtemanche, S. Nattel. (2002, Apr.). Time-dependent transients in an ionically based mathematical model of the canine atrial action potential. *Am. J. Physiol. Heart Circ. Physiol*. [Online]. 282 (4), pp. H1437-51. Available: <http://ajpheart.physiology.org/content/282/4/H1437.long>
- [14] V. M. García, A. Liberos, A.M. Vidal, M.S. Guillem, J. Millet, A. González, F.J. Martínez-Zaldívar, A.M. Climent. (2014, Jan.). Adaptive step ODE algorithms for the 3D simulation of electric heart activity with graphics processing units. *Comput Biol Med*. [Online]. 44 , pp. 15-26. Available: <http://www.sciencedirect.com/science/article/pii/S0010482513003107>
- [15] M. Rodrigo, A. M. Climent, A. Liberos, D. Calvo, F. Fernández-Avilés, O. Berenfeld, F. Atienza, M. S. Guillem. (2016, Aug.). Identification of Dominant Excitation Patterns and Sources of Atrial Fibrillation by Causality Analysis. *Ann Biomed Eng*. [Online]. 44 (8), pp. 2364-76. Available: <http://link.springer.com/article/10.1007%2Fs10439-015-1534-x>
- [16] R. S. MacLeod, C. R. Johnson, P. R. Ershler. (1991). Construction of an inhomogeneous model of the human torso for use in computational electrocardiography. *Conf Proc IEEE Eng Med Biol Soc*. [Online]. 12 (2), pp. 688-689. Available: <https://utah.pure.elsevier.com/en/publications/construction-of-an-inhomogeneous-model-of-the-human-torso-for-use>
- [17] M. S. Guillem, A. M. Climent, J. Millet, A. Arenal, F. Fernández-Avilés, J. Jalife, F. Atienza, O. Berenfeld. (2013, Apr.). Noninvasive

- localization of maximal frequency sites of atrial fibrillation by body surface potential mapping. *Circ Arrhythm Electrophysiol.* [Online]. 6 (2), pp. 294-301. Available: <http://circep.ahajournals.org/content/6/2/294.long>
- [18] F. Atienza, D. Calvo, J. Almendral, S. Zlochiver, K. R. Grzeda, N. Martínez-Alzamora, E. González-Torrecilla, A. Arenal, F. Fernández-Avilés, O. Berenfeld. (2011, Mar.). Mechanisms of fractionated electrograms formation in the posterior left atrium during paroxysmal atrial fibrillation in humans. *J Am Coll Cardiol.* 2011 Mar 1;57(9):1081-92.
- [19] P. A. Yushkevich, J. Piven, H. C. Hazlett, R. G. Smith, S. Ho, J. C. Gee, G. Gerig. (2006, Jul.). User-guided 3D active contour segmentation of anatomical structures: significantly improved efficiency and reliability. *Neuroimage.* [Online]. 31 (3), pp. 1116-28. Available: <http://www.sciencedirect.com/science/article/pii/S1053811906000632>
- [20] F. Remondino. (2004, Jan.). 3-D reconstruction of static human body shape from image sequence. *Computer Vision and Image Understanding.* [Online]. 93 (1), pp. 65-68. Available: <http://www.sciencedirect.com/science/article/pii/S1077314203001243>
- [21] D. W. Eggert, A. Lorusso, R. B. Fish. (1997). Estimating 3-D rigid body transformations: a comparison of four major algorithms. *Machine Vision and Applications.* [Online]. 9, pp. 272-290. Available: http://graphics.stanford.edu/~smr/ICP/comparison/eggert_comparison_mv97.pdf
- [22] C. Ramanathan, Y. Rudy. (2001, Feb.). Electrocardiographic imaging: II. Effect of torso inhomogeneities on noninvasive reconstruction of epicardial potentials, electrograms, and isochrones. *J Cardiovasc Electrophysiol.* [Online]. 12 (2), pp. 241-52. Available: <http://onlinelibrary.wiley.com/doi/10.1046/j.1540-8167.2001.00241.x/abstract>
- [23] B. J. Messinger-Rapport, Y. Rudy (1990, Apr.). Noninvasive recovery of epicardial potentials in a realistic heart-torso geometry. Normal sinus rhythm. *Circ Res.* [Online]. 66 (4), pp. 1023-39. Available: <http://circres.ahajournals.org/content/66/4/1023.long>
- [24] B. J. Messinger-Rapport, Y. Rudy (1986, Jul.). The inverse problem in electrocardiography: a model study of the effects of geometry and conductivity parameters on the reconstruction of epicardial potentials. *IEEE Trans Biomed Eng.* [Journal]. 33 (7), pp. 667-76.
- [25] M. S. Guillem, A. M. Climent, M. Rodrigo, F. Fernández-Avilés, F. Atienza, O. Berenfeld. (2016, Apr.). Presence and stability of rotors in atrial fibrillation: evidence and therapeutic implications. *Cardiovasc Res.* [Online]. 109 (4), pp. 480-92. Available: <http://cardiovascres.oxfordjournals.org/content/109/4/480.long>
- [26] B. J. Messinger-Rapport, Y. Rudy. (1989, Nov.). Computational issues of importance to the inverse recovery of epicardial potentials in a realistic heart-torso geometry. *Math Biosci.* [Online]. 97 (1), pp. 85-120. Available: <http://www.sciencedirect.com/science/article/pii/0025556489900448>
- [27] C. Ramanathan, Y. Rudy. (2001, Feb.). Electrocardiographic imaging: I. Effect of torso inhomogeneities on body surface electrocardiographic potentials. *J Cardiovasc Electrophysiol.* [Online]. 12 (2), pp. 229-40. Available: <http://onlinelibrary.wiley.com/doi/10.1046/j.1540-8167.2001.00229.x/abstract>
- [28] L. K. Cheng, J. M. Bodley, A. J. Pullan. (2003, Jan.). Effects of experimental and modeling errors on electrocardiographic inverse formulations. *IEEE Trans Biomed Eng.* [Online]. 50 (1), pp. 23-32. Available: <http://ieeexplore.ieee.org/document/1179128/>
- [29] A. Ferrer, R. Sebastián, D. Sánchez-Quintana, J. F. Rodríguez, E. J. Godoy, L. Martínez, J. Saiz. (2015, Nov.). Detailed Anatomical and Electrophysiological Models of Human Atria and Torso for the Simulation of Atrial Activation. *PLoS One.* [Online]. 10 (11), pp. e0141573. Available: <http://journals.plos.org/plosone/article?id=10.1371/journal.pone.0141573>
- [30] L. R. Bear, L. K. Cheng, I. J. LeGrice, G. B. Sands, N. A. Lever, D. J. Paterson, B. H. Smaill. (2015, Jun.). Forward problem of electrocardiography: is it solved? *Circ Arrhythm Electrophysiol.* [Online]. 8 (3), pp. 677-84. Available: <http://circep.ahajournals.org/content/8/3/677.long>
- [31] M. Rodrigo, M. S. Guillem, A. M. Climent, J. Pedrón-Torrecilla, A. Liberos, J. Millet, F. Fernández-Avilés, F. Atienza, O. Berenfeld. (2014, Sep.). Body surface localization of left and right atrial high-frequency rotors in atrial fibrillation patients: a clinical-computational study. *Heart Rhythm.* [Online]. 11 (9), pp. 1584-91. Available: <http://www.sciencedirect.com/science/article/pii/S154752711400544X>

Figueras

[Huiskamp, G. J.; van Oosterom, A., Heart position and orientation in forward and inverse electrocardiography. *Med Biol Eng Comput.* 30, 613-620, 1992](#)

[Jiang, Y.; Meng, Y.; Farina, D.; Dössel, O., Effect of respiration on the solutions of forward and inverse electrocardiographic problems – a simulation study. *Computers in Cardiology.* 36, 17-20, 2009](#)

[Keller, D. U. J.; Weber, F. M.; Seemann, G.; Dössel, O., Ranking the influence of tissue conductivities on forward-calculated ECGs. *IEEE Transactions on Biomedical Engineering.* 57, 1568-1576, 2010](#)

[van Dam, P. M.; van Oosterom, A., Volume conductor effects involved in the genesis of the P wave. *Europace* 7 suppl. 2, 30-38, 2005](#)

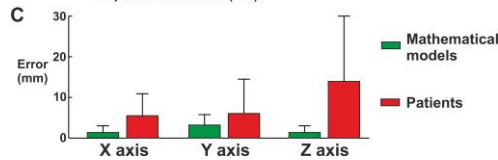
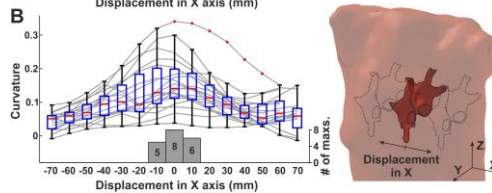
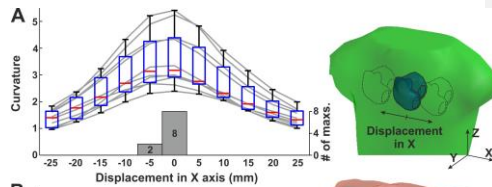
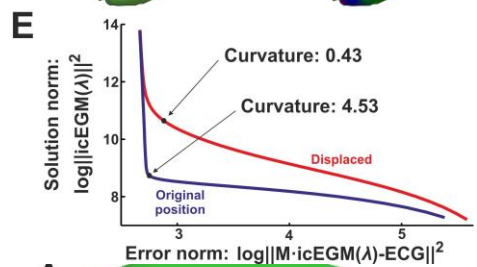
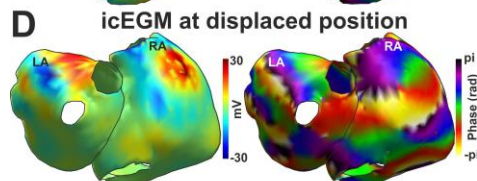
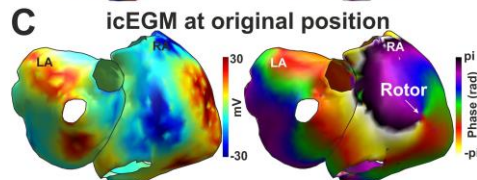
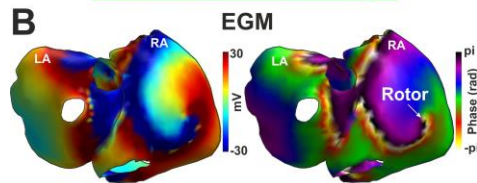
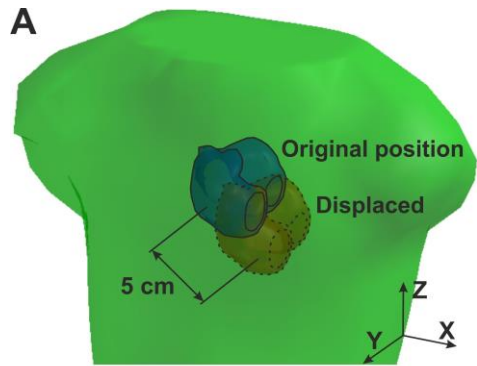


Fig. 2. Estimation of atrial position under displacements in X axis for (A) mathematical models and (B) patients. (C) Error in atrial position for independent displacements in the 3 axes. L-curve curvature for each simulation/patient (gray lines), boxplot of the curvature values for each displacement (blue) and number of maximal curvature in each displacement (gray bars).

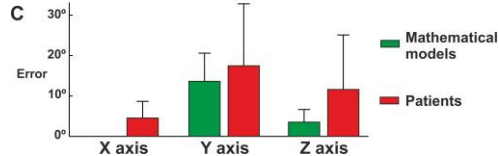
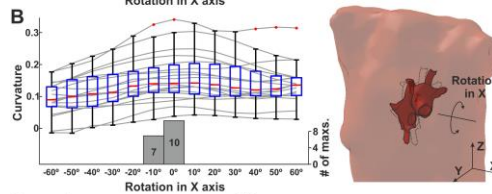
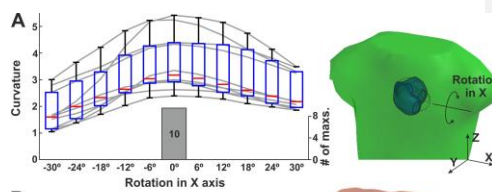


Fig. 3. Estimation of atrial orientation under rotations in X axis for (A) mathematical models and (B) patients. (C) Error in atrial orientation for independent rotations in the 3 axes. L-curve curvature for each simulation/patient (gray lines), boxplot of the curvature values for each rotation (blue) and number of maximal curvature in each rotation (gray bars).

